



Size effects in modeling diffusivity of hardened mortar

R.S.O. Keskin*, K.C. Hover, M. Grigoriu

School of Civil and Environmental Engineering, Cornell University, Ithaca, NY 14853, USA

ARTICLE INFO

Article history:

Received 1 March 2010

Accepted 25 February 2011

Keywords:

Effective diffusivity

Size effect

Random heterogeneous materials

Local method

Itô process

Chloride diffusivity of mortar specimens

ABSTRACT

A critical parameter for evaluating the resistance of concrete against chloride diffusion is effective diffusivity. While it can be obtained experimentally, this paper concerns computer simulations to estimate diffusivity of mortars as influenced by paste, aggregate, and interfacial effects. However, when performing such simulations, the size of the mortar sample modeled must be large enough to reliably characterize these randomly distributed effects, while remaining small enough for computational efficiency. The purpose of this paper is to report the influence of sample size on computed results and to recommend the smallest specimen size needed to obtain reliable estimates of diffusivity.

© 2011 Elsevier Ltd. All rights reserved.

1. Introduction

Reinforced concrete structures deteriorate in time due to various adverse conditions, e.g., chemical attacks and freeze–thaw cycles. Of the various deterioration mechanisms, chloride-induced corrosion of steel reinforcement bars is of great importance since numerous reinforced concrete structures are exposed to chloride sources, e.g., de-icing salts or marine environment. There are several mechanisms of chloride transport in concrete, e.g., diffusion and convection. In the absence of a high pressure head, diffusion dominates the transport in saturated concrete [1], and is of interest to this research. A critical parameter for evaluating the resistance of concrete against chloride diffusion is the effective diffusivity, which provides material-specific information on the rate of chloride transport through the material in question.

While measuring a macroscopic material property of a random heterogeneous material, specimen size needs to be large enough to represent statistically the property of interest. Since concrete is a random heterogeneous material, size effect needs to be considered in studying its effective properties. Bažant [2] and Huet [3] studied the size effect in modeling structural responses of heterogeneous materials comprehensively. In the context of this study, size effect in modeling mortar and concrete specimens that are used for estimating the effective diffusivity via computer simulations is of concern. Although the size effect on the structural and mechanical

properties of concrete has been studied extensively, the studies on size effect in modeling transport properties of concrete are fewer.

While performing computer simulations to obtain effective properties of random heterogeneous materials, errors may mainly result from: (i) statistical fluctuations, (ii) discretization, and (iii) finite size effects [4,5]. The magnitude of errors resulting from statistical fluctuations is related to the number of samples, which is usually determined by the available computational power. Discretization error is a result of representation of continuum media with discrete pieces. Zohdi and Wriggers [6] studied computational material testing, and presented an example illustrating the effect of mesh refining on the mechanical properties of a composite material. The method proposed in this study does not need to discretize the domain of interest.

Errors due to finite size effects are minimized by optimizing specimen size in such a way that the specimen is statistically representative of the material of interest. Specimen size for a random heterogeneous material can vary according to the property of interest when a fixed statistical error is aimed [7]. For a particular material property, the change in value of this property obtained from specimens of various dimensions can be used to approximate the size of the representative specimen [5,7,8]. For example, Quintanilla and Torquato [9] employed such a computer simulation method to study the probability distribution of the volume fraction for different models of random media. Roberts and Garboczi [4] determined the size of the computational cell used for studying the elastic properties of model porous ceramics by varying the cell size to map the size effect.

Accordingly, specimen size is a significant parameter in obtaining the effective diffusivity from either computer simulations or laboratory experiments. In general, disk-shaped specimens with a

* Corresponding author. Present address: Department of Civil Engineering, Yıldız Technical University, Esenler, Istanbul 34210, Turkey. Tel.: +90 532 653 3606; fax: +90 212 383 5133.

E-mail addresses: okeskin@yildiz.edu.tr (R.S.O. Keskin), kch7@cornell.edu (K.C. Hover), mdg12@cornell.edu (M. Grigoriu).

diameter of 100 mm and a thickness ranging from 10 mm to 50 mm are used in laboratory tests [10]. As explored in this paper, in the case of computer simulations, specimen size needs to be sufficiently small to reduce computational demand, but sufficiently large to obtain stable results. The required specimen size for obtaining reliable estimates of effective diffusivity is determined mainly by specimen to particle scale ratio. A well known method for estimating effective diffusivity of concrete via computer simulation was developed by Garboczi and Bentz [11], where computational concrete volumes of $30 \times 30 \times 30$ mm are filled with hard spheres, representing aggregate, surrounded with soft shells, representing transition zone between aggregate and cement paste. The spheres have diameters in the range of 0.075–19.05 mm, resulting in a specimen to particle scale ratio of 1.57.

This paper addresses the question, "How large should the model specimen be for a reliable estimate of effective diffusivity via computer simulation?". A probability-based numerical method that can be used for estimating the effective diffusivity was proposed in Refs. [12,13]. This paper presents a statistical study for identifying the smallest specimen size needed to obtain reliable estimates of effective properties. We are interested in the smallest specimen size with this property to minimize calculations. Caré's [14] experiments for measuring the effective diffusivities of mortar specimens were chosen as reference. Virtual 2D specimens of mortar were generated with target properties at microscale and their effective diffusivities were estimated. Based on the estimates obtained from specimens of various dimensions, specimen size was identified as at least the maximum sand particle diameter in the direction parallel to the simulated chloride flow and 20 times the maximum sand particle diameter in the orthogonal direction.

2. Virtual specimens

Mortar is a random heterogeneous material consisting of aggregate held together with a hardened cement paste. It is a three-phase material at microscale: aggregate, bulk cement paste and interfacial transition zone (ITZ). The ITZ surrounding an aggregate particle has a thickness up to 50 μm [15,16], and is characterized by higher porosity and coarser pores than those of the bulk cement paste remote from the aggregate surface [15–17]. Since the chloride transport within mortar takes place mainly through capillary pores [18], the ITZ may have an impact on the transport characteristics of mortar, depending on the microstructural differences between the ITZ and the bulk cement paste, and on their relative volumes. Therefore, a mortar specimen is represented by a random dispersion of virtual aggregate particles (of a given grain size distribution) surrounded by ITZs, with the remaining volume filled with bulk cement paste.

A methodology is proposed for representing and generating virtual 2D specimens. The methodology has three essential components [12], a probabilistic model for 2D aggregate particles, a Monte Carlo algorithm for generating virtual aggregate particles and an algorithm for placing virtual aggregate particles within a given container. When a particle is placed within the container, the ITZ is automatically defined at the periphery of the particle. After all particles are placed, the remaining space represents the bulk cement paste.

2.1. Aggregate model

As illustrated in Fig. 1, aggregate particles are represented in two dimensions by ellipses with random semi-axes, to which a random noise is added, so that the functional form of a 2D aggregate particle is

$$I(\theta) = R_1 \cos(\theta) + R_2 \sin(\theta) + g(R_1)Z(\theta), \quad \theta \in [0, 2\pi], \quad (1)$$

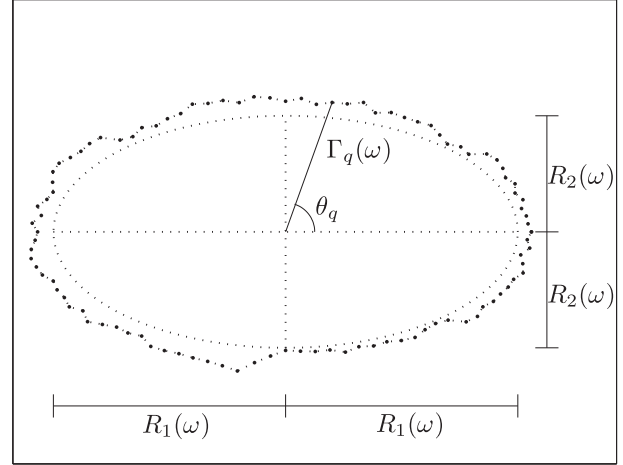


Fig. 1. Virtual particle.

where Γ is the radial distance between the boundary of the particle and the center of the underlying ellipse, R_1 and R_2 are the semi-major and -minor axes of the underlying ellipse, respectively, Z is a random field, θ is the angle (counter-clockwise) with respect to the major axis of the underlying ellipse and g is a function of R_1 which gives a positive scaling factor. R_1 and R_2 must be positive and bounded, and $Z(0, \omega)$ must be equal to $Z(2\pi, \omega)$ in order to have a closed shape.

Consider an interval $I = (i_1, i_{n_i+1}]$, $0 < i_1 < i_{n_i+1} < \infty$, and partition I into subintervals $I_k = (i_k, i_{k+1}]$, $k = 1, \dots, n_i$, $i_1 < i_2 < \dots < i_{n_i} < i_{n_i+1}$, where n_i is the number of subintervals. Suppose that conditional on $R_1 \in I_k$, R_1 is uniformly distributed on I_k . Then the probability distribution function of R_1 is

$$f_{R_1}(r_1) = \sum_{k=1}^{n_i} \mathbb{1}(r_1 \in I_k) \frac{p_k}{\lambda(I_k)}, \quad (2)$$

where

$$\lambda(I_k) = i_{k+1} - i_k, \quad (3)$$

$$p_k = P(R_1 \in I_k), \quad \sum_{k=1}^{n_i} p_k = 1. \quad (4)$$

Since $R_1 \in I_k = (i_k, i_{k+1}]$, $0 < i_k < i_{k+1} < \infty$, $k = 1, \dots, n_i$, R_1 is positive and bounded.

Let I_Σ denote an interval $(i_{\Sigma,1}, i_{\Sigma,2}]$, $0 < i_{\Sigma,1} < i_{\Sigma,2} \leq 1$. Suppose that Σ is a random variable uniformly distributed on I_Σ and independent of R_1 , and R_2 has the form given by

$$R_2 = \Sigma R_1, \quad (5)$$

so that R_2 is dependent on Σ and R_1 . Since Σ and R_1 are positive and bounded, R_2 is also positive and bounded.

Let the random field Z be defined by

$$Z(\theta) = F_Z^{-1} \circ \Phi(Y(\theta)), \quad \theta \in [0, 2\pi], \quad (6)$$

where F_Z is the beta distribution function with support $[0, 1]$ and shape parameters $\alpha_1 > 0$ and $\alpha_2 > 0$, Y is a stationary Gaussian field, independent of R_1 and R_2 , with mean 0 and variance 1, and Φ is the standard Gaussian distribution function. Z is a beta translation field, and its correlation function is completely defined by its marginal distribution and the covariance function of the underlying Gaussian field Y . The function g scales $Z \in [0, 1]$ (Eq. (1)), so that the resulting particle does not have an unrealistic shape.

Particles are stored in discretized forms in digital environments, so that Eq. (1) is replaced with

$$T_q = R_1 \cos(\theta_q) + R_2 \sin(\theta_q) + g(R_1)Z_q, \quad (7)$$

where $\theta_q = (q-1)\Delta\theta$, $\Delta\theta = 2\pi/n$, $q = 1, \dots, n+1$. $Z_q = F_Z^{-1} \circ \Phi(Y_q)$ is a coordinate of $(n+1)$ -dimensional vector $Z = [Z^{(1)} \ Z^{(2)}]^T$, where $Z^{(1)} = [Z_2 \ \dots \ Z_n]^T$ and $Z^{(2)} = [Z_1 \ Z_{n+1}]^T$. Z is an AR(1) model with lag one correlation coefficient $\rho \in (0, 1)$, i.e., the elements of its covariance matrix are $\rho^{|q_1-q_2|}$, $q_1, q_2 = 1, \dots, n+1$. Y_q is a coordinate of $(n+1)$ -dimensional Gaussian vector $Y = [Y^{(1)} \ Y^{(2)}]^T$ with zero mean and covariance matrix

$$\mathbf{c} = \begin{bmatrix} \mathbf{c}^{(1,1)} & \mathbf{c}^{(1,2)} \\ \mathbf{c}^{(2,1)} & \mathbf{c}^{(2,2)} \end{bmatrix}, \quad (8)$$

which is a rearranged AR(1) model covariance matrix. Partitions of \mathbf{c} are

$$c_{ij}^{(1,1)} = \rho^{|i-j|}, \quad i, j = 1, \dots, n-1, \quad (9a)$$

$$c_{i,1}^{(1,2)} = \rho^i, \quad i = 1, \dots, n-1, \quad (9b)$$

$$c_{1,i}^{(1,2)} = \rho^{n-i}, \quad i = 1, \dots, n-1, \quad (9c)$$

$$\mathbf{c}^{(2,1)} = (\mathbf{c}^{(1,2)})^T, \quad (9d)$$

$$c_{ij}^{(2,2)} = 1, \quad i=j=1, 2, \quad (9e)$$

$$c_{ij}^{(2,2)} = \rho^n, \quad i \neq j. \quad (9f)$$

The conditional vector $\tilde{\mathbf{Y}} = \mathbf{Y}^{(1)} | (\mathbf{Y}^{(2)} = \mathbf{y})$ is a $(n-1)$ -dimensional vector with mean matrix $\tilde{\mu} = \mathbf{c}^{(1,2)}(\mathbf{c}^{(2,2)})^{-1}\mathbf{y}$ and covariance matrix $\tilde{\mathbf{c}} = \mathbf{c}^{(1,1)} - \mathbf{c}^{(1,2)}(\mathbf{c}^{(2,2)})^{-1}\mathbf{c}^{(2,1)}$, where $\mathbf{y} = N(0, 1)[1 \ 1]^T$. Then $\tilde{\mathbf{Y}}$ can be given in the form

$$\tilde{\mathbf{Y}} = \tilde{\mu} + \beta\mathbf{G}, \quad (10)$$

where β is the Cholesky decomposition of $\tilde{\mathbf{c}}$, i.e., $\beta\beta^T = \tilde{\mathbf{c}}$, and \mathbf{G} is a standard Gaussian vector with independent and identically distributed coordinates.

2.2. Generation of virtual specimens

A virtual specimen is generated in two sequential stages. First, all particles are generated using the model presented in Section 2.1. Second, those particles are placed within a given container. When a particle is placed within the container, the ITZ is automatically defined at the periphery of the particle. ITZs are assumed to be of constant thickness, and are allowed to overlap. After all particles are placed within the container, the remaining space represents the bulk cement paste, and the generation of the virtual specimen is accomplished.

The codes for generating virtual specimens were developed under the MATLAB environment. Input parameters for generating a virtual specimen are particle size distribution, area fraction A_{agg} of particles, dimensions l_1 and l_2 of the container, shape parameters α_1 and α_2 of Z , the parameter ρ for constructing the covariance matrix of Y , and the interval $I_\Sigma = (i_{\Sigma,1}, i_{\Sigma,2}]$, $0 < i_{\Sigma,1} < i_{\Sigma,2} \leq 1$.

The particle size distribution is given in a form similar to that of an actual sieve analysis. Since particles are generated in two dimensions, it is assumed that they stand parallel to the orifices of sieves. The particle size distribution is described by the number n_i of sieves, the sizes $d_{L,k}$, $k = 1, \dots, n_i$, of the sieves and the proportion (by area) p_k of particles retained on each sieve, $\sum_{k=1}^{n_i} p_k = 1$. Particle diameter is the maximum distance between any two points on the boundary of a particle. A particle is retained on the sieve of size $d_{L,k}$ if its diameter is in the interval $I_k = (d_{L,k}, d_{U,k}]$, $0 < d_{L,k} < d_{U,k} < \infty$, where $d_{U,k}$ is the size of the upper sieve.

2.2.1. Particle generation

The target total area of the particles that will be retained on each sieve can be calculated as $A_k = p_k A_{\text{agg}} l_1 l_2$, $k = 1, \dots, n_i$, since p_k, A_{agg}, l_1

and l_2 are given as input. Let \hat{A}_k be the resulting total area of the particles that will be retained on the sieve of size $d_{L,k}$. After a particle that will be retained on the sieve of size $d_{L,k}$ is generated, \hat{A}_k is updated. Such particles are generated till \hat{A}_k exceeds A_k for the first time. Eventually, a collection of virtual particles in proportions \hat{p}_k , approximately equal to the target proportions p_k , is obtained.

The algorithm for generating a particle that will be retained on the sieve of size $d_{L,k}$ is outlined below (see Fig. 2).

- The subinterval I_k on which R_1 is assumed to be uniformly distributed is $(d_{L,k}/2, d_{U,k}/2]$. A semi-major axis $R_1(\omega) \in I_k$ is generated by using MATLAB's `rand` command as

$$R_1(\omega) = \frac{d_{L,k}}{2} + \text{rand}(1) \left(\frac{d_{U,k} - d_{L,k}}{2} \right). \quad (11)$$

- An axis ratio $\Sigma(\omega) \in I_\Sigma = (i_{\Sigma,1}, i_{\Sigma,2}]$ is generated by using MATLAB's `rand` command as

$$\Sigma(\omega) = i_{\Sigma,1} + \text{rand}(1)(i_{\Sigma,2} - i_{\Sigma,1}), \quad (12)$$

so that an ellipse with the semi-major axis of $R_1(\omega)$ and the semi-minor axis of $R_2(\omega) = \Sigma(\omega)R_1(\omega)$ is obtained.

- $\mathbf{Y}^{(2)}(\omega)$ is generated by using MATLAB's `randn` command as $\mathbf{Y}^{(2)}(\omega) = \text{randn}(2, 1)$.
- Since ρ is given, \mathbf{c} can be calculated from Eq. (9). Using \mathbf{c} and $\mathbf{Y}^{(2)}(\omega)$, $\tilde{\mu}(\omega)$ and $\tilde{\mathbf{c}}(\omega)$ are calculated. Then β can be obtained from the Cholesky decomposition of $\tilde{\mathbf{c}}$.
- $\mathbf{G}(\omega)$ is generated by using MATLAB's `randn` command as $\mathbf{G}(\omega) = \text{randn}(n-1, 1)$.
- $\tilde{\mathbf{Y}}(\omega)$ is calculated from Eq. (10).
- $\mathbf{Y}(\omega)$ is constructed using $\tilde{\mathbf{Y}}(\omega)$ and $\mathbf{Y}^{(2)}(\omega)$. Then $\mathbf{Z}(\omega)$ is obtained from Eq. (6) (memoryless transformation).
- Scaling factor is calculated by

$$g(R_1(\omega)) = \frac{d_{U,k}}{2} - R_1(\omega) \geq 0. \quad (13)$$

- The particle is obtained from Eq. (7) (Fig. 1).

2.2.2. Particle placement

After the particles are generated, they need to be placed at random locations within a container to generate a virtual specimen. The locations forming a random point field are generated by applying dependent thinning to a homogeneous Poisson field, and is called a Poisson hard-core field [19]. The particles are sequentially placed within the given rectangular container in a descending order according to the particle diameter, since there

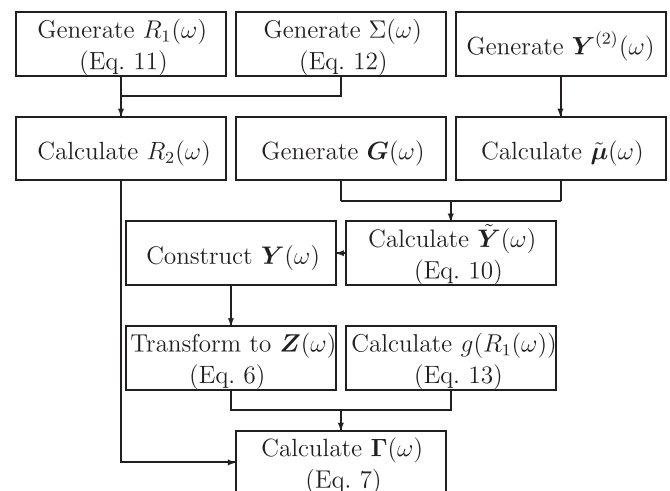


Fig. 2. Algorithm for generating a particle.

might not be enough space left for larger particles if smaller particles were placed first.

Let H denote a bounded rectangle whose lower-left corner coincides with the origin of \mathbb{R}^2 , i.e., $H = (0, l_1) \times (0, l_2)$, $l_1 > 0$, $l_2 > 0$. Suppose that the random point field N_h is a homogenous Poisson field. Conditional on $N_h(l_1, l_2) = n_h \geq n_p$, where n_p is the number of particles to be placed within H , the points of N_h are uniformly and independently distributed within H (Section 3.2, [19]), i.e., $V_{m,1} \sim U(0, l_1)$ and $V_{m,2} \sim U(0, l_2)$, $m = 1, \dots, n_h \geq n_p$, where $V_{m,1}$ and $V_{m,2}$ denote the coordinates of point m which belongs to N_h . Some points belonging to N_h may be rejected since it may not be possible to place particles at those points due to overlapping of particles. The remaining points form a Poisson hard-core field N_p , where $N_p(l_1, l_2) = n_p$. Let Λ_j be the initial orientation angle of particle j , $j = 1, \dots, n_p$. Λ_j is assumed to be uniformly distributed on $[0, 2\pi]$ and independent of the coordinates of the point at which particle j will be placed.

Suppose that $j - 1$ particles have already been placed within H and j th particle will be placed. The algorithm for placing particle j using MATLAB is outlined below (see Fig. 3).

- Λ_j is generated by using MATLAB's `rand` command as $\Lambda_j(\omega) = 2\pi \times \text{rand}(1)$.
- $(V_{m,1}(\omega), V_{m,2}(\omega))$, $m \geq j$, are generated by using MATLAB's `rand` command as $V_{m,1}(\omega) = l_1 \times \text{rand}(1)$ and $V_{m,2}(\omega) = l_2 \times \text{rand}(2)$.

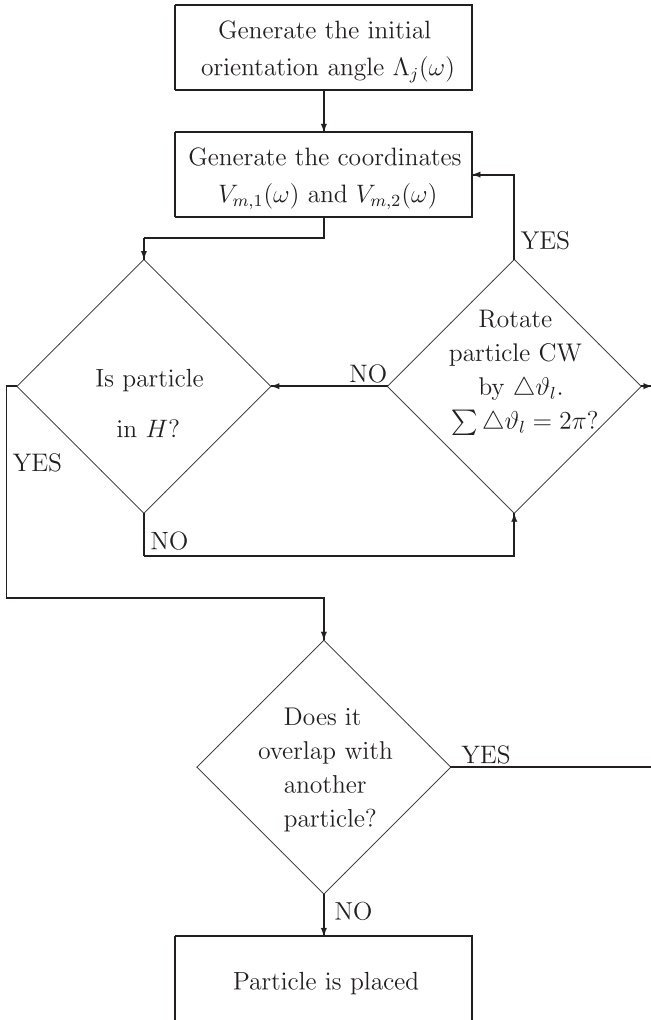


Fig. 3. Algorithm for placing a particle.

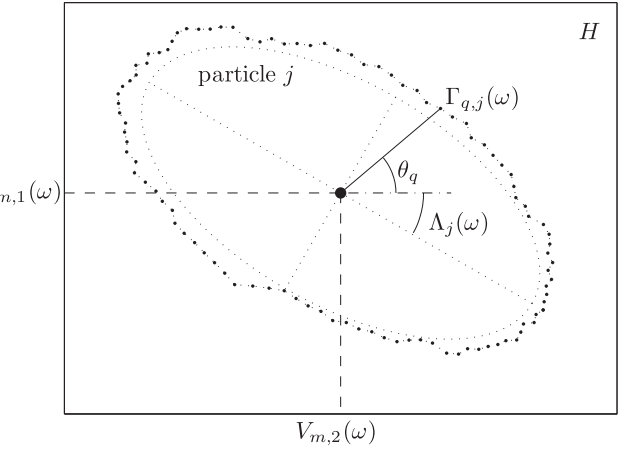


Fig. 4. Placing particle j .

- The particle is placed within H in such a way that the center of the underlying ellipse coincides with $(V_{m,1}(\omega), V_{m,2}(\omega))$. Then it is rotated clockwise by an amount of Λ_j (Fig. 4).
- A check is performed to determine whether the particle is within H or not, and whether the particle overlaps with a previously-placed particle within H . The details of the algorithm which checks overlapping can be found in Ref. [12]. If the particle is not within H and/or overlaps with another particle, it is rotated clockwise incrementally until it satisfies both conditions. If there is no orientation angle satisfying those conditions, a new point is generated, and the same procedure is followed.

2.3. Virtual test specimens

The essential difference between mortar and concrete is that in mortar the aggregate particle size distribution is finer, and the paste to aggregate volume ratio is higher. The work reported here is classified as mortar because the maximum size of the aggregate was limited to 2 mm to permit use of smaller simulation models and thus limit computational power and time. Just how small these models could be and still return reliable estimates of diffusivity is of course the central issue here. Further, since the area ratios on a random slice through a heterogeneous composite are approximately the same as the volume ratios in the parent 3D composite, the area ratios in the generated models matched volume fraction statistics of actual (3D) mixtures.

One of the actual mortar specimens physically tested by Caré [14] was chosen as a basis for generating virtual specimens. The sand particle size distribution in the mortar specimen of Caré [14] is plotted in Fig. 5. The proportions p_k , $k = 1, \dots, 6$, of particles retained on each sieve are shown in Table 1. The target area fraction of aggregate in the virtual specimens was likewise set to the volume fraction of aggregate in the mortar specimen of Caré [14], i.e., 50%.

In actual experiments, disk-shaped specimens are cut from cylindrical specimens. In order to simulate a similar procedure, a relatively large specimen is generated, and the specimens that will be used in analyses are cut from this specimen. Virtual specimens are labeled as $SP - l_1 \times l_2 - \omega_s$, $s = 1, \dots, n_{sp}$, where l_1 and l_2 are the dimensions parallel and orthogonal to the simulated chloride flow, respectively, and n_{sp} is the number of virtual specimen samples.

A virtual mortar specimen, $l_1 = 200$ mm by $l_2 = 100$ mm, was generated and labeled as $SP - 200 \times 100 - \omega_1$. The resulting proportions \hat{p}_k are shown in Table 1. The resulting area fraction \hat{A}_{agg} of 23,955 particles is 0.5001. The snapshots taken after the

particles retained on each sieve have been placed during the generation of SP – 200 × 100 – ω_1 are given in Figs. 6–11.

It should be noted that this algorithm – placing particles sequentially at random locations – is not suitable for generating specimens with high area fractions of particles. A few simulations targeting high area fractions were performed using the particle size distribution given in Table 1. The resulting specimens have area fractions of particles around 75% at most. A dynamic stage, in which particles are moved and rotated simultaneously after they are placed within a container, is needed to generate a specimen with a higher area fraction of particles; however, there is no need to employ such a dynamic stage in this study since the area fraction of particles is 50%. Also, a few simulations were run for various specimen to particle scale ratios targeting the same particle size distribution. The variation is higher for very low

specimen to particle scale ratios; however, the agreement is good in SP – 200 × 100 – ω_1 since the specimen to particle scale ratio is more than sufficient.

Three $l_1 = 10$ mm by $l_2 = 100$ mm specimens were cut from various locations of SP – 200 × 100 – ω_1 , and labeled as SP – 10 × 100 – ω_s , $s = 1, \dots, 3$ (Fig. 12). They have 1291, 1288 and 1294 particles, where the resulting area fractions of particles are 0.5042, 0.5014 and 0.5003, respectively. Similarly, three $l_1 = 2$ mm by $l_2 = 100$ mm specimens, SP – 2 × 100 – ω_s , $s = 1, \dots, 3$, were cut from SP – 10 × 100 – ω_1 , $s = 1, \dots, 3$, respectively. SP – 2 × 100 – ω_s , $s = 1, \dots, 3$, have 317, 337 and 326 particles, where the resulting area fractions of particles are 0.5025, 0.5049 and 0.5023, respectively.

The diffusivities in the aggregate particles, the bulk cement paste and the ITZ are needed for calculating the effective diffusivity of virtual specimens. They were assigned as follows (see Fig. 13).

- The aggregate particles are assumed to be nonporous.
- The bulk cement paste is assumed to have a constant diffusivity D_{cp} .
- The diffusivity in the ITZ is assumed to be described by

$$D(y) = c_1 y + c_2 y^2 + c_3 e^{-y}, \quad 0 < y \leq l_{ITZ}, \quad (14)$$

where y is the distance from the aggregate surface measured along the local normal, l_{ITZ} is the ITZ thickness, c_1 , c_2 and c_3 are some constants satisfying a presumed ratio $\alpha_D = D(0)/D(l_{ITZ})$, $\partial D(l_{ITZ})/\partial y = 0$ and $D(l_{ITZ}) = D_{cp}$.

For all virtual mortar specimens used in this study, D_{cp} , l_{ITZ} and α_D were chosen as $2.7 \cdot 10^{-6}$ mm²/s, 30 μm and 10, respectively. Then c_1 , c_2 and c_3 in Eq. (14) are –0.0016, 0.027 and $2.7 \cdot 10^{-5}$, respectively. Likewise, a constant value for thickness of the ITZ was used at the periphery of all aggregate particle sizes, and for all simulations compared here.

3. Effective diffusivity

The effective diffusivity of a specimen of heterogeneous material is defined as the diffusivity of a fictitious homogeneous specimen with the same global properties as those of the original heterogeneous specimen. It is shown in Refs. [12,13] that the effective diffusivities of deterministic and random heterogeneous specimens can be calculated using a local method presented in Ref. [20]. A brief review of the method is given here.

Let $H = (0, l_1) \times (0, l_2) \in \mathbb{R}^2$ be a bounded subset containing a virtual mortar specimen (Fig. 14). The chloride concentration $C(\mathbf{x})$ satisfies

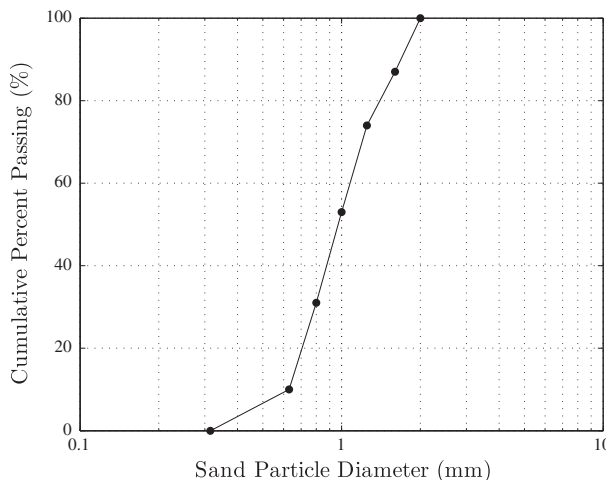


Fig. 5. Sand particle size distribution [14].

Table 1
Particle size distribution in virtual specimens.

$d_{L,k}$ (mm)	$d_{U,k}$ (mm)	p_k (by area)	\hat{p}_k (by area)
0.315	0.630	0.10	0.10
0.630	0.800	0.21	0.21
0.800	1.000	0.22	0.22
1.000	1.250	0.21	0.21
1.250	1.600	0.13	0.13
1.600	2.000	0.13	0.13

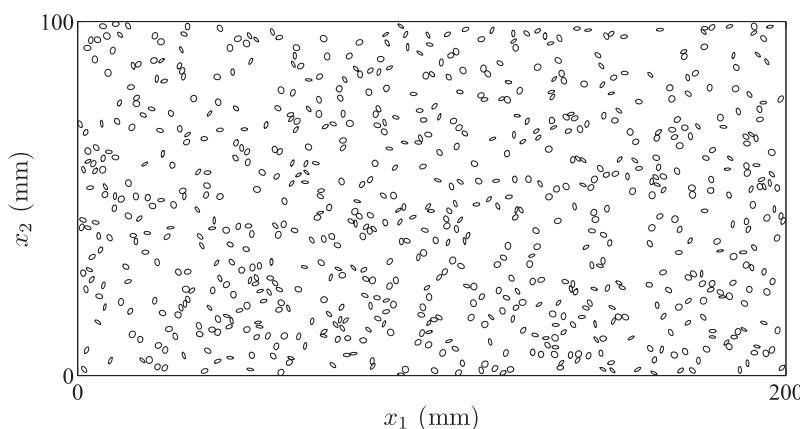


Fig. 6. SP – 200 × 100 – ω_1 (753 particles).

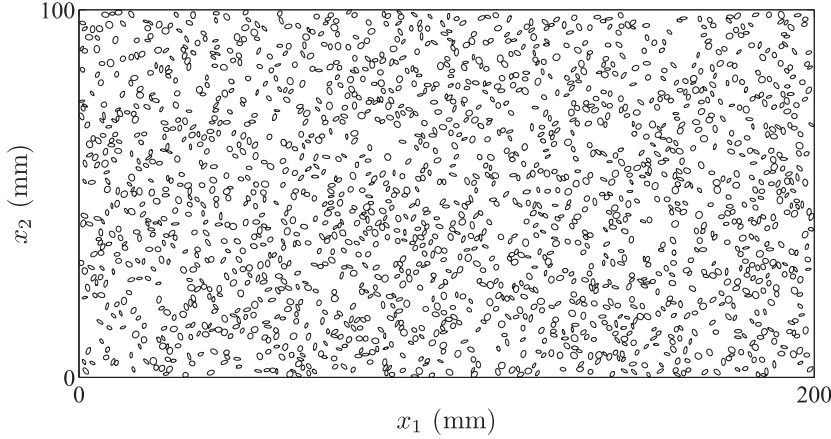


Fig. 7. SP – 200 × 100 – ω_1 (1916 particles).

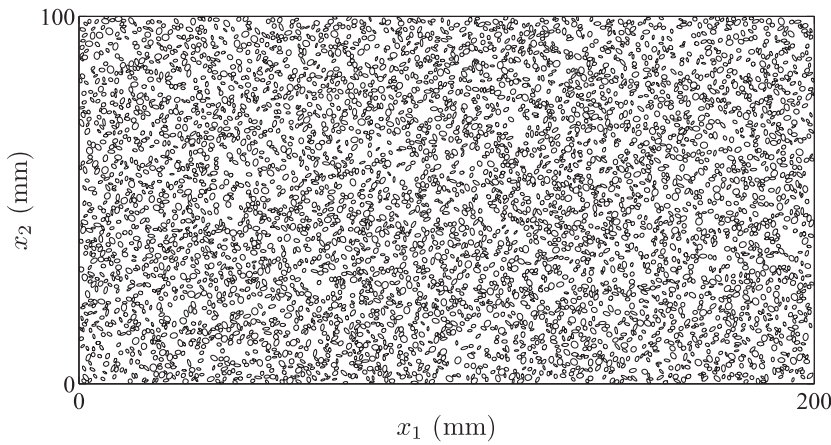


Fig. 8. SP – 200 × 100 – ω_1 (4979 particles).

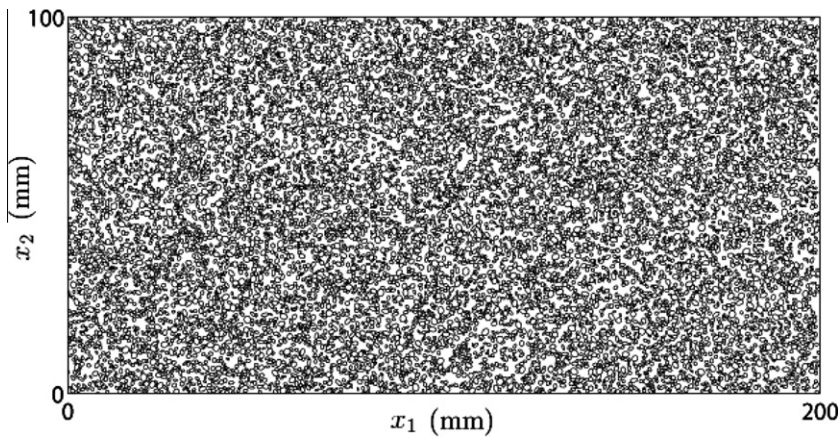


Fig. 9. SP – 200 × 100 – ω_1 (10,022 particles).

$$\sum_{p=1}^2 \frac{\partial D(\mathbf{x})}{\partial x_p} \frac{\partial C(\mathbf{x})}{\partial x_p} + D(\mathbf{x}) \Delta C(\mathbf{x}) = 0, \quad \mathbf{x} \in H, \quad (15)$$

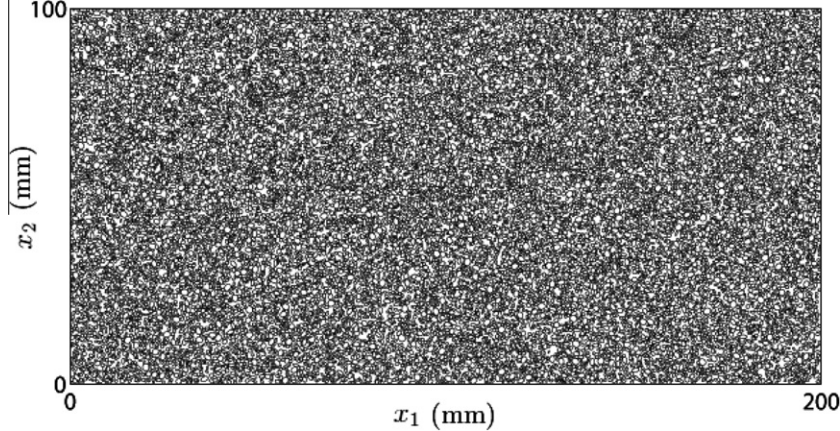
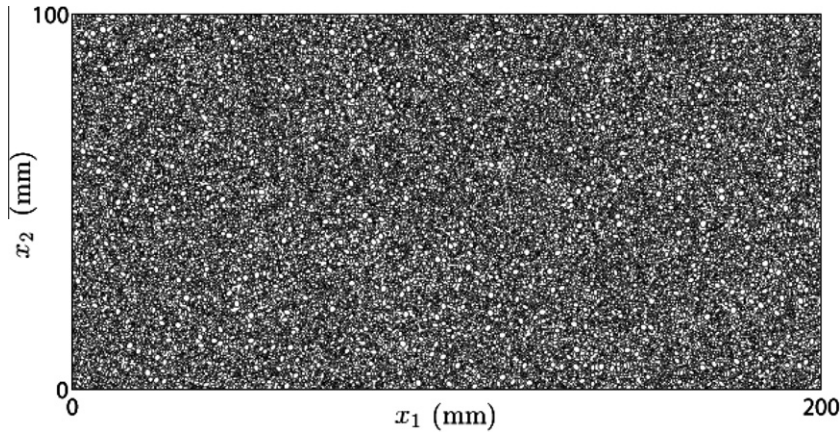
where $D(\mathbf{x})$ is the diffusivity at \mathbf{x} and Δ is the Laplace operator, with the Dirichlet boundary conditions

$$C(0, x_2) = 0 \quad \text{and} \quad C(l_1, x_2) = 1, \quad x_2 \in (0, l_2), \quad (16)$$

and the Neumann boundary conditions

$$\frac{\partial C(\mathbf{x})}{\partial x_2} = 0, \quad \mathbf{x} \in (0, l_1) \times \{0\} \quad \text{and} \quad \mathbf{x} \in (0, l_1) \times \{l_2\}. \quad (17)$$

Eqs. (16) and (17) are the boundary conditions of a steady-state chloride diffusion experiment. The boundary $\{l_1\} \times (0, l_2)$ is exposed to a chloride solution with a unit concentration, while the boundary

Fig. 10. SP – 200 × 100 – ω_1 (17,558 particles).Fig. 11. SP – 200 × 100 – ω_1 (23,955 particles).

$\{0\} \times (0, l_2)$ is exposed to a solution free of chloride. Since the boundaries $(0, l_1) \times \{0\}$ and $(0, l_1) \times \{l_2\}$ are sealed, the chloride concentration at those boundaries are unknown, but the gradient of chloride concentration normal to those boundaries is zero. It is assumed that $D(\mathbf{x})$ and $D(\mathbf{x})/\partial x_p$ are continuous such that the solution of Eq. (15) exists and is unique.

An approximation to the effective diffusivity D_{eff} is given in Refs. [12,13] as

$$D_{\text{eff}} \simeq \frac{l_1}{l_2} \sum_{k=1}^{n_2} D(l_1 - \zeta, x_{2,k}) \frac{1 - C(l_1 - \zeta, x_{2,k})}{\zeta} \Delta x_{2,k}, \quad (18)$$

where ζ is the distance between the integration points and the boundary $\{l_1\} \times (0, l_2)$, n_2 is the number of integration points on the line $(l_1 - \zeta) \times \{x_2\}$, $x_2 \in (0, l_2)$, and $\Delta x_{2,k}$, $k = 1, \dots, n_2$ is the incremental length corresponding to the point $x_{2,k}$. The unknowns in Eq. (18) are $C(l_1 - \zeta, x_{2,k})$, $k = 1, \dots, n_2$, which can be calculated using a local method [12,13].

The local solution of Eq. (15) is given in Refs. [12,13] as

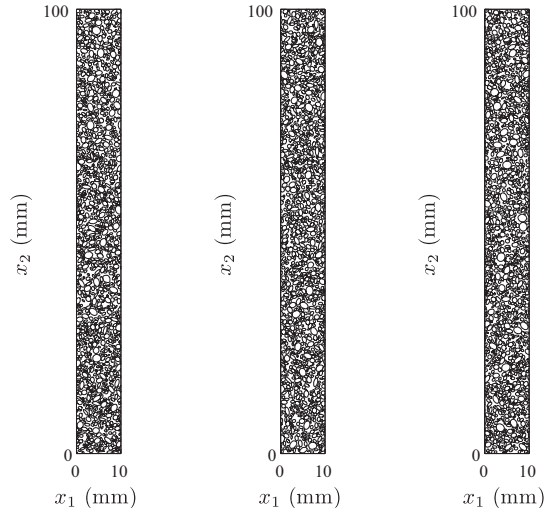
$$C(\mathbf{x}) = E[C(\tilde{\mathbf{X}}(\tilde{T}))], \quad (19)$$

where $\tilde{\mathbf{X}}$ is a \mathbb{R}^2 -valued process and

$$\tilde{T} = \inf\{\tau > 0 : \tilde{\mathbf{X}}(\tau) \notin H\} \quad (20)$$

is a stopping-time, i.e., the time at which $\tilde{\mathbf{X}}$ exits H for the first time. Let \mathbf{X} be a \mathbb{R}^2 -valued Itô process starting at $\mathbf{X}(0) = \mathbf{x}$. \mathbf{X} is defined by

$$d\mathbf{X}(\tau) = \mathbf{a}(\mathbf{X}(\tau))d\tau + \mathbf{b}(\mathbf{X}(\tau))dB(\tau), \quad \tau \geq 0, \quad (21)$$

Fig. 12. SP – 10 × 100 – ω_s , $s = 1, \dots, 3$.

where \mathbf{a} and \mathbf{b} are called drift and diffusion coefficients, respectively. If they are bounded functions satisfying the uniform Lipschitz conditions, the solution of Eq. (15) exists and is unique [21]. $\tilde{\mathbf{X}}$ is obtained by reflecting the \mathbb{R}^2 -valued Itô process \mathbf{X} at the Neumann boundaries $(0, l_1) \times \{0\}$ and $(0, l_1) \times \{l_2\}$, that is, $\tilde{\mathbf{X}} = [\tilde{X}_1 = X_1, \tilde{X}_2 = r(X_2)]$, where $r(u)$ is a periodic function with period $2l_2$

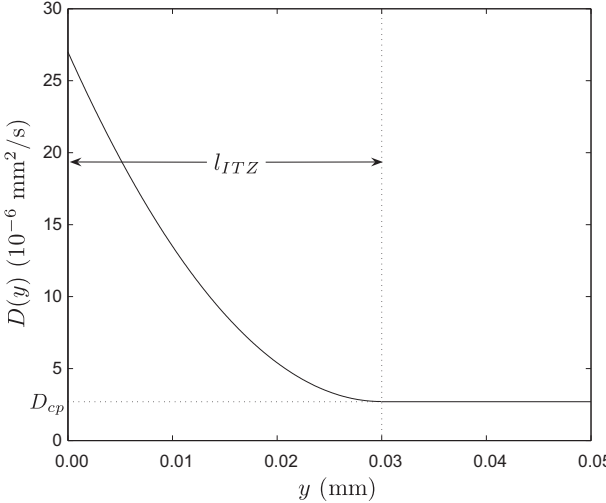


Fig. 13. Diffusivity in the ITZ.

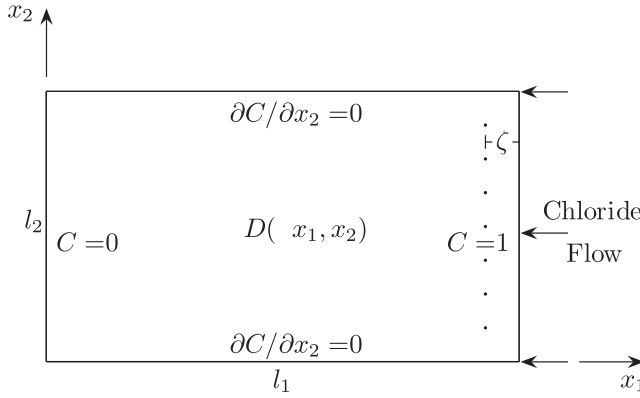


Fig. 14. Virtual test specimen.

coinciding with $|u|$ for $u \in [-l_2, l_2]$. The drift and diffusion coefficients are supposed to have the form

$$a_1(\mathbf{x}) = \frac{\partial D(\tilde{\mathbf{x}})}{\partial \tilde{\mathbf{x}}_1}, \quad a_2(\mathbf{x}) = r'(x_2) \frac{\partial D(\tilde{\mathbf{x}})}{\partial \tilde{\mathbf{x}}_2}, \quad \mathbf{b}(\mathbf{x}) = \sqrt{2D(\tilde{\mathbf{x}})} \mathbf{i}, \quad (22)$$

where $\mathbf{x} \in (0, l_1) \times \mathbb{R}$ and $\tilde{\mathbf{x}} \in H$. Even though $r(x_2)$ is not differentiable at $x_2 = kl_2$, $k \in \mathbb{Z}$, it can be shown that the process $\tilde{\mathbf{X}}$ can solve Eq. (15) locally by using arguments similar to the ones used in Ref. [21] (Section 6.2.3.2) for extending Tanaka's formula to the case of Brownian motions reflected at two thresholds.

Since it is not possible to calculate the expectation in Eq. (19) analytically except for few cases, $C(\mathbf{x})$ is estimated by

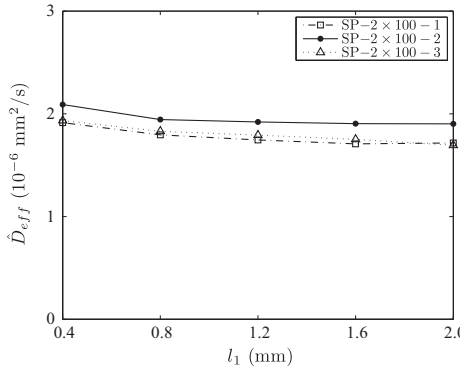


Fig. 15. D_{eff} vs. specimen size $(0, l_1) \times (0, 100)$.

$$\widehat{C}(\mathbf{x}) = \frac{1}{\tilde{n}_s} \sum_{l=1}^{\tilde{n}_s} C(\tilde{\mathbf{X}}(\tilde{T}(\omega), \omega)) = \frac{\tilde{n}'_s}{\tilde{n}_s}, \quad (23)$$

where \tilde{n}_s and \tilde{n}'_s are the total number of samples of $\tilde{\mathbf{X}}$ and the number of samples of $\tilde{\mathbf{X}}$ that exit H through the Dirichlet boundary $\{l_1\} \times (0, l_2)$ [12,13].

4. Determination of specimen size

The objective is to minimize l_1 and l_2 such that reliable estimates of the effective diffusivity can still be obtained. A two-stage procedure is proposed to determine the specimen size. First, the dimension l_1 parallel to the simulated chloride flow, second, the dimension l_2 orthogonal to the simulated chloride flow are minimized. The analysis procedure is given in Appendix A.

4.1. Determining l_1

In order to minimize l_1 , l_1 needs to be sufficiently large that the resulting estimates of the effective diffusivity are independent of l_2 . Intuitively, l_2 was chosen as 50 times the maximum sand particle diameter, i.e., $l_2 = 100$ mm. The specimens are presented in Section 2.3.

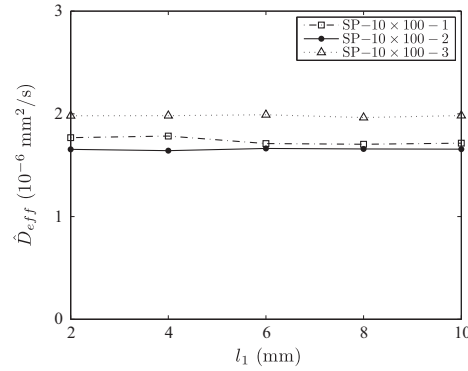
For $l_2 = 100$ mm, \widehat{D}_{eff} was calculated from Eq. (18) for increasing l_1 until stable estimates of the effective diffusivity were obtained. Computationally, it means to find stopping time (Eqs. (A.1) and (A.2)) as a function of l_1 , the number n_2 of integration points and the distance ζ between the integration points and the boundary $\{l_1\} \times (0, l_2)$.

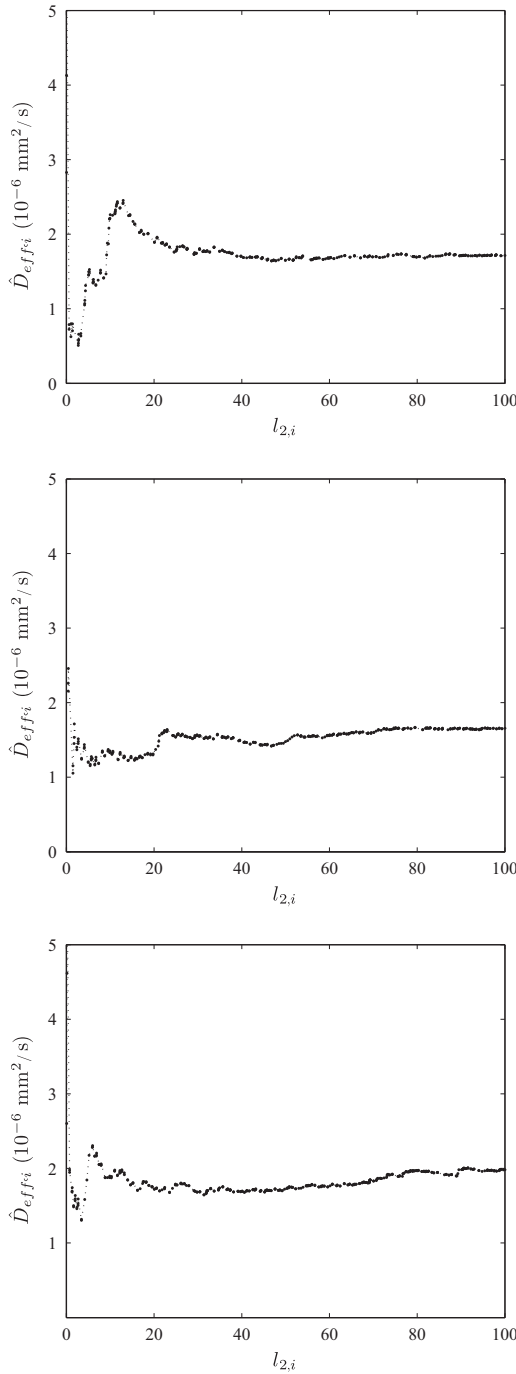
The resulting estimates of the D_{eff} for $l_1 = 2 - 0.4 \cdot (j-1)$ and $l_1 = 10 - 2 \cdot (j-1)$, $j = 1, \dots, 5$ are plotted in the left and right panels of Fig. 15, respectively. The estimates are stable for l_1 greater than 2 mm, which corresponds to the maximum sand particle diameter. As l_1 decreases beyond 2 mm, the estimates increase gradually.

It is worthy to note that when a specimen with l_1 equal to the maximum particle size is cut from a larger specimen, the probability of a particle of maximum size lying fully across the cut-specimen is low, so that $l_1 = 2$ mm can be considered as a conservative value.

4.2. Determining l_2

In order to minimize l_2 , the results obtained for $SP - 10 \times 100 - s$, $s = 1, \dots, 3$, in the previous section were used, rather than solving Eq. (15) for various values of l_2 . Estimates of the D_{eff} for various values of l_2 were calculated by

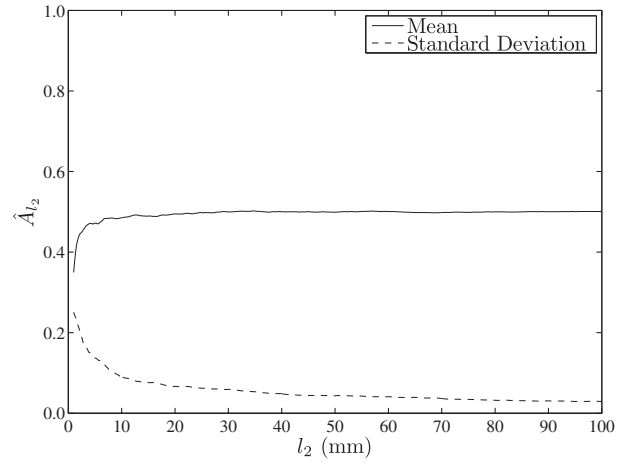


Fig. 16. D_{eff} vs. specimen size $(0, 10) \times (0, l_2)$.

$$\hat{D}_{\text{eff}} = \frac{l_1}{l_2} \sum_{k=1}^j \Delta x_{2,k} D(l_1 - \zeta, x_{2,k}) \frac{1 - \hat{C}(l_1 - \zeta, x_{2,k}, \omega)}{\zeta}, \quad (24)$$

where $l_1 = 10$ mm, $\zeta = 0.5$ mm, l_2 was determined by the value of $j = 1, \dots, n_2$ and the values of $\hat{C}(l_1 - \zeta, x_{2,k}, \omega)$ were taken from the analyses of SP – 10 × 100 – ω_s , $s = 1, \dots, 3$. Fig. 16 shows the evolution of \hat{D}_{eff} with l_2 . It can be observed from Fig. 16 that \hat{D}_{eff} stabilizes with l_2 greater than 40 mm.

A critical parameter for determining the value of l_2 is the fraction of the line $\{l_1 - \zeta\} \times (0, l_2)$ falling into aggregate, denoted as A_{l_2} . Estimates of mean and standard deviation of A_{l_2} as a function

Fig. 17. Estimates of mean and standard deviation of A_{l_2} .

of l_2 are shown in Fig. 17. The estimates are based on 150 samples from SP – 200 × 100 – 1, i.e., $\{x_1\} \times (0, 100)$, $x_1 = 26, \dots, 175$.

It is important to note that the evaluation of the results assumes that errors related to the use of a finite number of samples of X , a finite time interval $\Delta\tau$ and a reduced number of integration points $x_{2,k}$, $k = 1, \dots, n_2$ are small relative to those related to specimen size. The number of samples was determined by investigating how many samples are sufficient to obtain stable estimates [13]. Time interval was set to a value that enables a sample to explore the entire specimen (Appendix A). The number of integration points was determined by an algorithm that selects points according to the diffusivity profile (Appendix A).

4.3. Size effect

The estimates of the effective diffusivity obtained from specimens of various sizes validate the fact that size effect needs to be considered in calculating/measuring the effective diffusivity of mortar and concrete. Possible reasons of size effect are that

- (i) the fraction of aggregate may differ from the target fraction of aggregate as the specimen gets smaller,
- (ii) if a specimen is too narrow in the direction parallel to the simulated chloride flow, it is possible for an aggregate to lie across the specimen, causing the ITZ, in which the diffusivity is relatively high, to percolate the specimen,
- (iii) the tortuosity of diffusion paths in small specimens may not represent the actual tortuosity, which may cause non-uniform diffusion at shallow depths of mortar and concrete specimens.

5. Conclusion

A statistical study for identifying the smallest specimen size needed to obtain reliable estimates of effective diffusivity using the method proposed in Refs. [12,13] was conducted. The specimens tested by Caré [14] were chosen as the reference. Virtual 2D specimens of mortar were generated with target properties at microscale and the effective diffusivities of those specimens were estimated.

The results suggest that specimen size needs to be determined with regard to aggregate particle size. The smallest specimen size for obtaining reliable estimates of the effective diffusivity of the given mortar was identified as $l_1 = 2$ mm in the direction x_1 of chloride flow and $l_2 = 40$ mm in the orthogonal direction x_2 . Since a limited number of specimens were used in the simulations, a

conservative specimen size, $l_1 = 5$ mm by $l_2 = 50$ mm, resulting in ratios $l_1/(\text{maximum aggregate particle diameter}) = 2.5$ and $l_2/(\text{maximum aggregate particle diameter}) = 25$, was chosen for further analyses, which consider the calibration of parameters defining the diffusivity in the ITZ and the prediction of the effective diffusivity based on those calibrated parameters.

Based on the results obtained for mortar, l_1 can be chosen as 15–20 mm for generating virtual concrete specimens. Since the direction of the simulated flow is along the x_1 -axis and the boundaries parallel to the x_1 -axis are reflective, it is not necessary to constrain the ratio l_1/l_2 . Instead, l_2 can be chosen as 100 mm, which is a common value used in actual experiments, for generating virtual concrete specimens. In three-dimensional case, virtual specimens can be generated as disks with thickness l_1 and diameter l_2 since 2D specimens are generated using volume fraction statistics obtained from 3D specimens. Moreover, diffusion paths in the 3D specimen are likely to be more tortuous than those in the 2D specimen.

The method is stable and accurate, however, the accuracy depends on how realistic the diffusivities of the phases – aggregate, cement paste and ITZ – are defined. This study is a first step for employing the probability-based method presented by Grigoriu and Papoulias [20] to estimate the effective diffusivity of mortar, and the model does not incorporate microcracks or debonding of ITZs, which are likely to be present in a real specimen even if it is unloaded. Further studies on improving the model should consider cracks, voids and strain history of the specimen since they affect the diffusivity of mortar [22–24]. Such effects can be taken into account by properly defining the diffusivity within the specimen since one of the advantages of the model is that there is no need to discretize the specimen; however, it should be kept in mind that the diffusivity and its first order derivatives with respect to space are supposed to be continuous for the solution of Eq. (15) exists and is unique.

Acknowledgements

This research was conducted using the resources of the Cornell University Center for Advanced Computing, which receives funding from Cornell University, New York State, the National Science Foundation, and other leading public agencies, foundations, and corporations.

Appendix A. Calculation of \hat{D}_{eff}

The procedure for estimating D_{eff} by using the method given in Section 3 is outlined below.

- Choose a value for the distance ζ between the integration points and the boundary $\{l_1\} \times (0, l_2)$. It was chosen as 0.1 mm and 0.5 mm for analyses of $\text{SP} - 2 \times 100 - \omega_s$, $s = 1, \dots, 3$, and $\text{SP} - 10 \times 100 - \omega_s$, $s = 1, \dots, 3$, respectively.
- Determine the number n_2 and the vertical coordinates $x_{2,k}$, $k = 1, \dots, n_2$, of the integration points for each specimen. Using equally, or almost equally, spaced integration points may cause a significant error in the resulting estimate of the effective diffusivity because such a configuration of integration points may poorly represent the diffusivity profile along the line $\{l_1 - \zeta\} \times (0, l_2)$. Since aggregate particles are assumed to be nonporous, there is no need to place an integration point inside an aggregate particle. Moreover, the diffusivity in the ITZ is variable, while the diffusivity in the bulk cement paste is constant (Fig. 13), therefore, more closely spaced integration points are needed in the ITZ. If the integration points are determined according to the diffusivity profile along the line

$\{l_1 - \zeta\} \times (0, l_2)$, the selected points will be unevenly distributed and the number of points in any two specimens may be different. Such an algorithm is given in Ref. [12]. The values of n_2 for $\text{SP} - 2 \times 100 - \omega_s$, $s = 1, \dots, 3$, and $\text{SP} - 10 \times 100 - \omega_s$, $s = 1, \dots, 3$ were determined as 383, 460, 461, 317, 337 and 326, respectively.

- Define stopping times to obtain estimates of the D_{eff} for various values of l_1 . For $\text{SP} - 2 \times 100 - \omega_s$, $s = 1, \dots, 3$, five stopping times were set as

$$T_j = \inf\{\tau \geq 0 : \tilde{\mathbf{X}}(\tau) \notin (0.4 \cdot (j-1), 2) \times (0, 100)\}, \quad (\text{A.1})$$

where $j = 1, \dots, 5$, so that estimates of the D_{eff} could be obtained for $l_1 = 2 - 0.4 \cdot (j-1)$. Similarly, for $\text{SP} - 10 \times 100 - \omega_s$, $s = 1, \dots, 3$, five stopping times were set as

$$T_j = \inf\{\tau \geq 0 : \tilde{\mathbf{X}}(\tau) \notin (2 \cdot (j-1), 10) \times (0, 100)\}, \quad (\text{A.2})$$

where $j = 1, \dots, 5$, so that estimates of the D_{eff} could be obtained for $l_1 = 10 - 2 \cdot (j-1)$.

- Generate \tilde{n}_s samples of \mathbf{X} starting from each integration point in each specimen and obtain samples of $\tilde{\mathbf{X}} = [\tilde{X}_1 = X_1, \tilde{X}_2 = r(X_2)]$. It is shown in Ref. [13] that $\tilde{n}_s = 1000$ is sufficient to obtain stable estimates. Samples of \mathbf{X} were generated by using Euler's scheme, i.e.,

$$\mathbf{X}(\tau + \Delta\tau) \simeq \mathbf{X}(\tau) + \mathbf{a}(\mathbf{X}(\tau))\Delta\tau + \mathbf{b}(\mathbf{X}(\tau))\Delta\mathbf{B}(\tau), \quad (\text{A.3})$$

where $\tau \geq 0$, $\Delta\tau$ is time step and $\Delta\mathbf{B}(\tau)$ is the Brownian motion increment. A balance between the drift and diffusion contributions, $\mathbf{a}(\tilde{\mathbf{X}}(\tau))\Delta\tau$ and $\mathbf{b}(\tilde{\mathbf{X}}(\tau))\Delta\mathbf{B}(\tau)$, of the increment $\Delta\tilde{\mathbf{X}}(\tau) = \tilde{\mathbf{X}}(\tau + \Delta\tau) - \tilde{\mathbf{X}}(\tau)$ in $[\tau, \tau + \Delta\tau]$ should be maintained in order for $\tilde{\mathbf{X}}(\tau)$ to explore the entire specimen. The orders of magnitudes of these contributions are $\|\mathbf{a}(\tilde{\mathbf{X}}(\tau))\|\Delta\tau$ and $\|\mathbf{b}(\tilde{\mathbf{X}}(\tau))\mathbf{i}\|\sqrt{\Delta\tau}$, respectively. Suppose that $\tilde{\mathbf{X}}(\tau)$ belongs to ITZ, in which $D(\mathbf{x})$ varies rapidly, so that $\|\mathbf{a}(\tilde{\mathbf{X}}(\tau))\|$ is large. To assure that $\tilde{\mathbf{X}}(\tau)$ explores ITZ, $\Delta\tau$ needs to be reduced significantly such that the contributions of drift and diffusion are similar, and $\|\Delta\tilde{\mathbf{X}}(\tau)\|$ is smaller than the thickness of ITZ. After a few trials, $\Delta\tau$ was chosen as 1.5 s when $\tilde{\mathbf{X}}(\tau, \omega)$ belongs to ITZ and 15 s when it belongs to bulk cement paste. The resulting estimates of mean and standard deviation of $\|\Delta\tilde{\mathbf{X}}(\tau, \omega)\|$ are 12 μm and 11 μm , respectively. It is important to note that $\Delta\tau$ needs to be reduced as an aggregate surface is approached in order to avoid stepping into the aggregate particle, which is a non-diffusive phase.

- Based on samples of $\tilde{\mathbf{X}}$, calculate $\hat{C}(l_{1,j} - \zeta, x_{2,k}, \omega)$, $k = 1, \dots, n_2$, from Eqs. (23), (A.1) and (A.2) for each specimen.
- Calculate estimates of the D_{eff} by introducing $l_{1,j}$ and $\hat{C}(l_{1,j} - \zeta, x_{2,k}, \omega)$, $k = 1, \dots, n_2$, into Eq. (18).

References

- [1] Poulsen E, Mejlibro L. Diffusion of chloride in concrete – theory and application. New York: Taylor & Francis; 2006.
- [2] Bažant ZP. Probabilistic modeling of quasibrittle fracture and size effect. In: Corotis RB, Schueler GI, Shinozuka M, editors. Proceedings of the 8th international conference on structural safety and reliability (ICOSSAR), held at Newport Beach, Cal., Swets & Zeitinger; 2001. p. 1–23.
- [3] Huet C. Application of variational concepts to size effects in elastic heterogeneous bodies. J Mech Phys Solids 1990;38(6):813–41.
- [4] Roberts AP, Garboczi Ej. Elastic properties of model porous ceramics. J Am Ceram Soc 2000;83(12):3041–8.
- [5] Garboczi Ej, Bentz DP. The effect of statistical fluctuation, finite size error, and digital resolution on the phase percolation and transport properties of the NIST cement hydration model. Cement Concrete Res 2001;31:1501–14.
- [6] Zohdi TI, Wriggers P. Computational micro-macro material testing. Arch Comput Methods Eng 2001;8(2):131–228.
- [7] Stroeven M, Askes H, Sluys LJ. Numerical determination of representative volumes for granular materials. Comput Methods Appl Mech Eng 2004;193:3221–38.
- [8] Bear J. Eight lectures on mathematical modelling of transport in porous media. In: Bear J, Buchlin JM, editors. Modelling and applications of transport phenomena in porous media. Dordrecht: Kluwer Academic Publishers; 1991. p. 1193. Chapter 1.

- [9] Quintanilla J, Torquato S. Local volume fraction fluctuations in random media. *J Chem Phys* 1997;106(7):2741–51.
- [10] Stanish KD, Hooton RD, Thomas MDA. Testing the chloride penetration resistance of concrete: a literature review. FHWA Contract, DTFH61-97-R-00022. University of Toronto, Toronto, ON, Canada; 1997.
- [11] Garboczi EJ, Bentz DP. Multiscale analytical/numerical theory of the diffusivity of concrete. *Adv Cement Based Mater* 1998;8(2):77–88.
- [12] Keskin RSO. A probability-based numerical method for estimating effective diffusion coefficient in concrete. PhD thesis, Cornell University, Ithaca, NY; 2008.
- [13] Keskin RSO, Grigoriu M. A probability-based method for calculating effective diffusion coefficients in composite media. *Probab Eng Mech* 2010;25(2):249–54.
- [14] Caré S. Influence of aggregates on chloride diffusion coefficient into mortar. *Cement Concrete Res* 2003;33(7):1021–8.
- [15] Ollivier JP, Maso CJ, Bourdette B. Interfacial transition zone in concrete. *Adv Cement Based Mater* 1995;2(1):30–8.
- [16] Scrivener KL, Crumbie AK, Laugesen P. The interfacial transition zone (ITZ) between cement paste and aggregate in concrete. *Interfacial Sci* 2004;12(4):411–21.
- [17] Bentur A, Cohen MD. Effect of condensed silica fume on the microstructure of the interfacial zone in portland cement mortars. *J Am Ceram Soc* 1987;70(10):738–43.
- [18] Garboczi EJ. Permeability, diffusivity and microstructural parameters: a critical review. *Cement Concrete Res* 1990;20(4):591–601.
- [19] Sobczyk K, Kirkner DJ. Stochastic modelling of microstructures. Boston: Birkhäuser; 2001.
- [20] Grigoriu M, Papoulias KD. Effective conductivity by a probability-based local method. *J Appl Phys* 2005;98(3):1–10.
- [21] Grigoriu M. Stochastic calculus: applications in science and engineering. Boston: Birkhäuser; 2002.
- [22] Samaha HR, Hover KC. Influence of microcracking on the mass transport properties of concrete. *ACI Mater J* 1992;89(4):416–24.
- [23] Ismail M, Toumi A, François R, Gagné R. Effect of crack opening on the local diffusion of chloride in cracked mortar samples. *Cement Concrete Res* 2008;38(8–9):1106–11.
- [24] Kamali-Bernard S, Bernard F. Effect of tensile cracking on diffusivity of mortar: 3D numerical modelling. *Comput Mater Sci* 2009;47(1):178–85.